

Received September 25, 2019, accepted October 18, 2019, date of publication October 29, 2019, date of current version November 12, 2019.

Digital Object Identifier 10.1109/ACCESS.2019.2950348

Adaptive Sequentially Weighted Median Filter for Image Highly Corrupted by Impulse Noise

JIAYI CHEN¹, YINWEI ZHAN², (Member, IEEE), AND HUIYING CAO¹

¹School of Information Engineering, Guangdong Medical University, Zhanjiang 524023, China

²School of Computer Science and Technology, Guangdong University of Technology, Guangzhou 510006, China

Corresponding author: Yinwei Zhan (ywzhan@ieee.org)

This work was supported in part by the National Natural Science Foundation of China under Grant 61170320, in part by the Guangdong Provincial Science and Technology Program in China under Grant 2017B010110015, in part by the Project of Science and Technology Program of Guangzhou in China under Grant 201604016034, and in part by the Medical Scientific Research Foundation of Guangdong Province in China under Grant B2018190.

ABSTRACT To tackle the difficulties in the detection and removal of impulse noise faced by the existing filters, and to further improve the denoising performance, we propose an adaptive sequentially weighted median filter for image corrupted by impulse noise. In the proposed method, a noise detector employing the 3σ principle of normal distribution and the local intensity statistics, is proposed; and a sequentially weighted median filter with a neighborhood of adaptive size, is proposed for noise removal, in which the weighted operator is derived in reference to the spatial distances from central noisy pixel, i.e., the weighting coefficients are sequentially inversely proportional to the spatial distances. The experimental results confirm that the proposed method outperforms the existing filters, excelling in the capability of noise removal, structure and edge information preservation.


INDEX TERMS Image denoising, median filter, noise detection, noise removal, sequentially weighted median filter, 3σ principle.

I. INTRODUCTION

An image is often corrupted by impulse noise in the process of acquisition and transmission; and there are two types of impulse noise: fixed-valued impulse noise and random-valued impulse noise [1]. Fixed-valued impulse noise is also called salt and pepper noise, one most common noise in images; it severely impacts the image processing and analysis, such as image recognition, segmentation, and so on. Therefore, effective removal of impulse noise is highly needed. For removal of fixed-valued impulse noise, the mean filter [2] and median filter [3] were originally proposed. However, mean filter was found unable to preserve the structure and edge information of image, while median filter is preferred because of its simple processing and good performance. But thereafter, the traditional median filter was found unable to obtain a thorough noise removal and structure information preservation simultaneously, especially for high density noise, because it processes all pixels regardless of whether they are noisy or not, destroying the noise free pixels. To address this problem, some researchers initially proposed

switching median filters [4]–[7] that integrate the noise removal processing with a noise detector so as to make the removal processing imposed only on the detected noisy pixels so that the performance of median filter was improved considerably. And in the wake of development of image processing, analysis, and application, the better denoising performance of filters is highly demanded; thus, various improved filters integrated with various strategies were proposed. However, the existing filters inevitably have inherent shortcomings, and are not necessarily effective, especially for high density noise: they either overly smooth the image, or are unable to restore effectively the structure and edge information, so that they still could not satisfy the high requirements of image analysis and application. To tackle this problem and provide high quality image for analysis and application, we proposed an adaptive sequentially weighted median filter (ASWMF) for image highly corrupted by impulse noise; the contributions of the proposed ASWMF are briefly described as follows.

(i) A noise detector employing the 3σ principle of normal distribution and the local intensity statistics based on the intensity distribution of natural image, taking full advantage of intensity distribution features to discriminate accurately

The associate editor coordinating the review of this manuscript and approving it for publication was Halil Ersin Soken .

the noisy pixels from the noise free ones having the same intensity.

(ii) A noise removal method employing sequentially weighted median of neighborhood of adaptive size; the weighted operator employed is derived in reference to the spatial distances from central noisy pixel, in which the weighting coefficients are sequentially inversely proportional to the spatial distances, distinguishing accurately the various contributions and impacts of neighbor pixels on the central noisy pixel according to the distances.

The rest of this paper is organized by several parts as follows. Section II states the related works, followed by the proposed method detailed in section III; the experiments and result analyses are conducted in section IV; and section V concludes this paper.

II. RELATED WORKS

For improving the standard median filter, researchers proposed switching median filters [4]–[7], which discriminate the noisy pixels from the noise free ones prior to the noise removal processing, so as to only make the detected noisy pixels undergo noise removal processing and keep the noise free ones unchanged. Comparatively, the switching median filters protect the original information of noise free pixels. However, switching median filters are unable to handle various density of noise. Considering this issue, adaptive switching median filters [8]–[11] were proposed; they are robust for various density of impulse noise. Wang et al. [10] proposed a novel learning-based switching median filter which detects noise by a learning-based method, and by an iterative manner, takes the median of noise free pixels surrounding noisy pixel as the estimated intensity of noisy pixel. However, its improved performance is achieved at the expense of computational complexity. Erkan et al. [11] proposed a different applied median filter (DAMF) to protect the thin lines and edges of image, and avoid smearing image details while removing noise; the DAMF employs the noise free pixels in a neighborhood of adaptive size for noise removal, and uses previously processed pixels to remove the residual noises.

In order to further improve the performance with various strategies, decision based filters [12], [13] were proposed; their robust strategies improve the noise detection accuracy and the performance of noise removal. A modified decision based unsymmetric trimmed median filter [12] proposed a noise detector identifying impulse noise simply by the extreme intensity; the detected noisy pixels are replaced by the unsymmetric trimmed median of a neighborhood of fixed size. A neighborhood decision based impulse noise filter (NDBINF) in [13] employs a neighborhood decision approach to protect the noise free pixels having extreme intensity while detecting noise, and a first-order neighborhood decision approach to restore the detected noisy pixels.

It is generally believed that mean filters are unable to achieve good performance, for they go without the ability of structure and edge information preservation; however, the improved variants of mean filter may get remarkable

results, especially for high density noise, such as [14], [15]. In [15], the intensity estimation of noisy pixel is performed by an adaptive weighted mean based on Euler distance; it is claimed by the authors that this filter can achieve excellent noise removal and good edge preservation. Apart from this, mean filter integrated with median filter may achieve better performance, such as [16]–[18]. In [18], the filter using pixel-variation gain factors (PVGf) groups the neighbor pixels having non-extreme intensity according to the intensity variation, and then, the distribution ratio and pixel variation level of each group are employed to determine the gain factors; thereafter, the value obtained by the gain factors multiplied with the median of each group is taken as the estimated intensity of noisy pixel.

As improved versions of switching median or mean filter, weighted filters [19]–[24] remove impulse noise by taking the weighted median or mean of neighbor noise free pixels with a weighted operator, differentiating the contributions and impacts of neighbor pixels on the central pixel by weighted processing so as to achieve a better denoising result. The adaptive dynamically weighted median filter (ADWMF) [22] estimates the intensity of noisy pixel by employing the weighted median of a neighborhood of adaptive size; the weighted operator employed is derived from Gaussian surface. The filter using radial basis functions interpolation (RBFi) in [24] estimates the intensity of noisy pixel with radial basis functions interpolation, and then, refines the recovery image using a distance inversely weighted mean filter.

In view of the wide application of fuzzy theory, it was introduced into the image processing for improving the denoising performance [25]–[28]. The SVM classification based fuzzy filter (SVMFF) [25], aiming at performance improvement irrespective of noise density, employs a support vector machine classification for noise detection, along with a histogram based fuzzy filtering for noise removal. Inspired by the fuzzy switching median filters and the works on the concept of information sets, a noise adaptive information set based switching median filter (NAISM) is proposed in [27]; the information sets are derived from fuzzy sets to deal with the uncertainty, and by virtue of the switching criterion and the local effective information surrounding the noisy pixel, the best calculated value replaces the noisy pixel.

Generally, existing techniques strongly rely on exploiting the neighbor information of noisy pixel for noise removal; however, considering the diversity singularity and non-stationary feature of image signal in local neighborhood, the estimation result could easily diverge from the true value and cause ugly visual effects in textures and edge regions. These inspired some researchers to expect better denoising performance by exploiting the nonlocal information during the noise removal procedure. However, initially, the nonlocal techniques were only for removal of additive Gaussian noise and random-valued impulse noise [29]; and subsequently, some researchers ingeniously proposed the improved versions of nonlocal techniques for fixed-valued impulse

noise removal. Wang et al. [30] proposed an iterative nonlocal means filter (INLM); the concept of nonlocal means filter is based on the fact that there exist lots of similar patches with repeat patterns in natural image, and the central pixels of these similar patches share the same intensity value distribution; the central noisy pixel under processing is thus replaced by the weighted mean of central pixels of all similar patterns. In general, the nonlocal filters show high computational complexity, and performance improvements for fixed-valued impulse noise are not necessarily conspicuous.

Originally, the deep learning technique based filters focused on Gaussian noise removal; thereafter, inspired by the emerging deep learning theories, some researchers attempted to use them for fixed-valued impulse noise, such as [31], [32]. When the noise is additive Gaussian, the noisy image value is still correlated to the original value, hence, deep learning based filter can achieve a good performance for Gaussian noise removal. However, unlike Gaussian noise, impulse noise is not correlated with the original image data, each pixel has a probability of being corrupted; thus, the deep learning based filters are not fit for impulse noise removal, also, by observing their experimental results in [31], [32], their performances are not conspicuous.

III. PROPOSED METHOD

A. MODEL OF FIXED-VALUED IMPULSE NOISE

Generally, the fixed-valued impulse noise can be modeled by its intensity and distribution. (i) Impulse noise takes extreme intensity in the image intensity range; in an 8-bit gray image whose intensity ranges from 0 to 255, the impulse noise takes intensity 0 and 255. (ii) When corrupts an image, the impulse noise distributes randomly and evenly with a certain probability, being independent from neighbor noise free pixels; the noises with minimum intensity and the ones with maximum intensity distribute with equal probability. Correspondingly, the impulse noise can be mathematically modeled as

$$f(p) = \begin{cases} \min & d/2 \\ \max & d/2 \\ o & 1 - d \end{cases} \quad (1)$$

Here, $f(p)$ is the intensity of pixel p in corrupted image with a noise density d , extreme values \min and \max denote the intensity of noisy pixel, and o denotes the intensity of noise free pixel.

B. NOISE DETECTION BY 3σ PRINCIPLE AND LOCAL STATISTICS

1) FEATURES OF FIXED-VALUED IMPULSE NOISE

To reveal the features of impulse noise as well as the distinction between noisy pixel and noise free pixel, a simple experiment is carried out, and the results are shown in FIGURE 1. FIGURE 1 shows a zoomed-in local part of image Lenna, which locates at 135~154 rows and 220~239 columns, and its corrupted versions by 10%, 50%, and 90% noises, respectively. By observing the corrupted

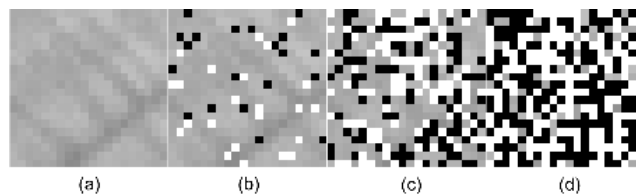


FIGURE 1. Zoomed-in local part of Lenna and its corrupted versions. (a) A local part of original image Lenna; corrupted versions by (b) 10% noises; (c) 50% noises; (d) 90% noises.

versions carefully, several important observations can be obtained as follows.

- (i) Fixed-valued impulse noise takes extreme intensity, i.e., 0 and 255.
- (ii) Noises with minimum intensity and noises with maximum intensity distribute randomly but local unevenly with equal probability.
- (iii) Local noise free pixels vary smoothly, and smooth regions are separated by edges.
- (iv) For noisy pixel, its intensity differs greatly from those of neighbor noise free pixels surrounding it, it is thus in isolation.
- (v) There are often some noise blocks in highly corrupted image.

2) NOISE DETECTOR BASED ON 3σ PRINCIPLE AND LOCAL STATISTICS

For a natural image, it can be noted from its intensity histogram that generally, the intensities of pixels approximately obey normal distribution, and so does the intensities of local pixels. The local noise free pixels have high similarity, and are highly correlated with each other, so that they approximately obey local normal distribution. And the noisy pixels take fixed extreme intensity, and their locations obey random distribution; thus, they are lonely, deviating considerably from the neighbor noise free pixels.

Naturally, based on the intensity feature of impulse noise, assuming all pixels having extreme intensity to be noisy, may not be valid, as the noise free pixels having extreme intensity are definitely taken as noisy pixels by this assumption. To address this problem, we seek help from the normal distribution.

Based on the just above analyses, we employ the 3σ principle of normal distribution for further detection, with the expectation that the noise detector has good ability to discriminate noise free pixels from the noisy ones having the same intensity value. As shown in FIGURE 2, denote by μ the mean of a set, and σ the standard deviation, if the individuals X of the set obey normal distribution, then 68.26% individuals would locate in interval $(\mu - \sigma, \mu + \sigma)$, 95.44% individuals locate in interval $(\mu - 2\sigma, \mu + 2\sigma)$, and 99.74% individuals locate in interval $(\mu - 3\sigma, \mu + 3\sigma)$; they can be defined by

$$\begin{aligned} P\{\mu - \sigma < X < \mu + \sigma\} &= 68.26\% & (2) \\ P\{\mu - 2\sigma < X < \mu + 2\sigma\} &= 95.44\% & (3) \\ P\{\mu - 3\sigma < X < \mu + 3\sigma\} &= 99.74\% & (4) \end{aligned}$$

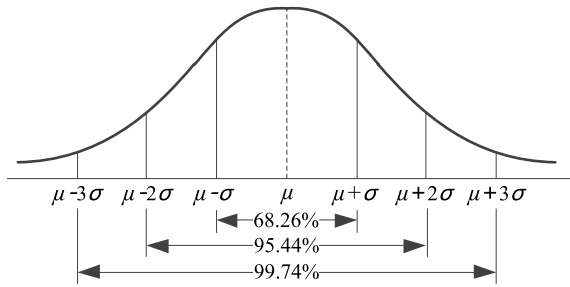


FIGURE 2. 3σ principle of normal distribution.

Note that one pixel with extreme intensity means high probability of being noisy, because of the extreme intensity feature of impulse noise; but if it locates in the 1σ interval shown in FIGURE 2 and formula (2), we take it as noise free, for it shows high correlation with the neighbor pixels having non-extreme intensity.

However, in a black or white region, noise detection by the extreme intensity and the 3σ principle of normal distribution fails; but fortunately, the features of black or white region can be inferred and utilized for noise detection. For example, for a black region, two important observations can be made as follows.

- (i) Originally, most or all the pixels in this black region take minimum intensity.
- (ii) When impulse noise corrupts this region, the noises with minimum intensity disappear for they are assimilated, only the noises with maximum intensity exist. Accordingly, it is noteworthy that most of pixels in this corrupted region are of minimum intensity.

Therefore, in a black image region, we employ local intensity statistics for noise detection based on these two observations, that is, if a pixel takes minimum intensity, and the minimum intensity accounts for the majority in its neighborhood, this pixel is labeled as noise free, otherwise as noisy. The noise detection strategy can be similarly made for a white region.

In addition, by reference to the literatures, and based on the approximate local symmetry of the pixels in spatial distribution, we take square neighborhood, which is symmetrical about the center, for noise detection and removal; we denote by $N_p(k)$ the neighborhood of size $k \times k$ centered at pixel p .

Specifically, the proposed noise detector based on 3σ principle and local intensity statistics is defined as follows.

- (i) Take the pixels having extreme intensity as noise candidates, because of the intensity feature of impulse noise.
- (ii) For each noise candidate p , in $N_p(7)$, if more than two non-extreme values are available, turn to (iii), or else, turn to (iv).
- (iii) Compute the mean u and standard deviation σ of the non-extreme intensity in $N_p(7)$; if $f(p)$ falls into interval $(u - \sigma, u + \sigma)$, label p as noise free, otherwise as noisy.
- (iv) In $N_p(5)$, if $f(p) = 0$ and the number of intensity 0 (denoted by n_0) accounts for the majority, here we set $n_0 > T$, label p as noise free, otherwise as noisy. This strategy is similar for $f(p) = 255$.

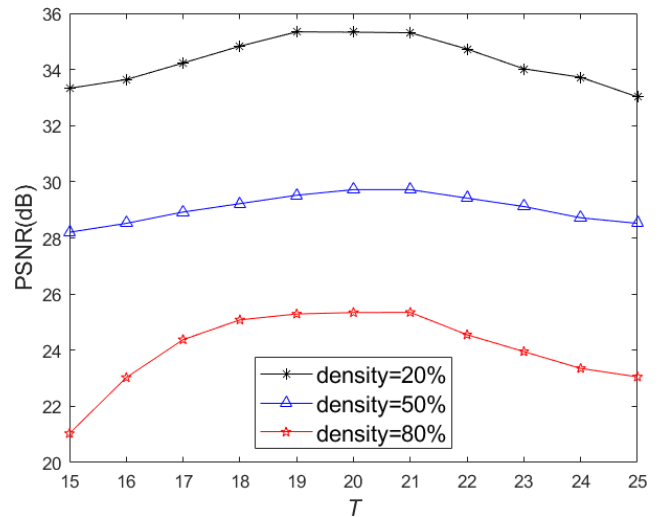


FIGURE 3. PSNR of ASWMF with various T on BSD68 dataset corrupted with various density of impulse noise.

For the optimal value of T , by using vast trial and error methods, we conducted an experiment with ASWMF on *BSD68* dataset corrupted with 20% noises, 50% noises, and 80% noises, respectively, the result of which is shown in FIGURE 3. The result shows how the denoising performance depends on the noise detector with various values of T . Based on the result, we prefer to take $T = 20$, which means the following formula should be approximately satisfied

$$\left. \frac{\partial \text{PSNR}(T)}{\partial T} \right|_{T=20} = 0 \tag{5}$$

The performance of an impulse noise detector depends on its capability to detect all the true positives effectively in the presence of false positives as less as possible. And the proposed noise detector is able to achieve this so that the edge and structure information can thus be better preserved and restored in the noise removal processing.

C. NOISE REMOVAL BY ADAPTIVE SEQUENTIALLY WEIGHTED MEDIAN

In our method, only the noisy pixels undergo a noise removal processing, and noise free pixels are left unchanged so as to protect the original image information as much as possible; in addition, for one noisy pixel, only the noise free pixels surrounding itself are employed in its intensity estimation. Besides, we employ a neighborhood of adaptive size for noise removal processing, i.e., if no noise free pixels are available in small neighborhood for noise removal processing, the neighborhood is enlarged so as to contain noise free pixels.

In our noise removal processing, noise free pixels only on the border of one neighborhood are employed. Take FIGURE 4 for an example. For the central noisy pixel p , initially, its $N_p(3)$ neighborhood is employed, and thus, noise free pixels only on the border of $N_p(3)$ are employed; and if no noise free pixels are available in the $N_p(3)$ for noise removal, the $N_p(5)$ is employed, in this case, equally, noise free pixels only on the border of $N_p(5)$ are employed, for no noise free pixels

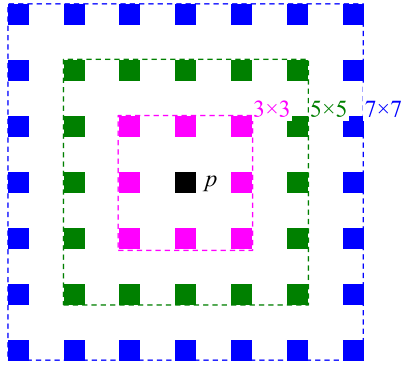


FIGURE 4. Neighborhood of adaptive size.

are available in the $N_p(3)$ which is also included in $N_p(5)$. However, the noise free pixels on the border of one neighborhood are not equidistant, and therefore, their contributions and impacts on the central pixel are unequal so that directly taking the median of them as the estimated intensity of central noisy pixel is partial and inadvisable. To differentiate the contributions and impacts of neighbor noise free pixels on the central pixel, the noise free pixels available on the border of one neighborhood, are weighted by a weighted operator, and then, the median of the weighted ones is taken as the intensity of noisy pixel under consideration.

Our weighted operator is innovatively defined in FIGURE 5, in which denoted by $W(k)$ the weighted operator of size $k \times k$. Note that in $W(k)$, the non-zero coefficients, by which the corresponding pixels are duplicated so as to control their probability of becoming the median, are sequentially inversely proportional to their spatial distances from central pixel, and are signed only to the noise free pixels at the corresponding locations, representing accurately the contributions and impacts of neighbor pixels on the central pixel. In addition, it is noteworthy that the coefficients assigned to noisy pixels are zero, for noisy pixels could not participate in the intensity estimation of central noisy pixel.

As mentioned above, if no noise free pixels are available, the neighborhood is enlarged until at least one noise free pixel is found or the neighborhood size has reached the predefined maximum. At this point, if the neighborhood has reached the maximum size, and still no noise free pixels are available, the noisy pixel under consideration is replaced by the median of all pixels in its neighborhood $N(5)$, including the pixels of previously processed, unprocessed, and noise free. As to the maximum size of neighborhood employed for noise removal, denote it by $MaxN$; it could not be too large, for pixels at far distance show weak correlation and impact, also, it could not be too small, for it shows no robustness for high density noise. By conducting experiments on various images and using trial and error method, we see that our proposed method with $MaxN=9$ and $MaxN=11$ shows almost the same best denoising performance; thus, we prefer to take 9 as the optimal value of $MaxN$, because of computational complexity.

In summary, the adaptive sequentially weighted median filter is set forth as follows. Each detected noisy pixel p undergoes the following adaptive weighted median processing.

(i) If noise free pixels are available on the border of $N_p(k)$ (initially, $k = 3$ is taken) under consideration, turn to (ii), or else, turn to (iii).

(ii) Conduct weighted processing on the noise free pixels by the weighted operator $W(k)$, and take the median of weighted ones as the intensity of p , which can be formulated as

$$f(p) = \text{median}(N_p(k) \diamond W(k)) \tag{6}$$

where the symbol \diamond is the pixel-wise duplication operator; for example, for a noise free pixel p with weighted coefficient n , the weighted processing is defined by

$$f(p) \diamond n = \overbrace{f(p), f(p), f(p), \dots, f(p)}^{n \text{ times}} \tag{7}$$

(iii) Enlarge the $N_p(k)$, i.e. set $k = k+2$; if $k \leq MaxN$, turn to (i), or else, let p unprocessed.

(iv) After processing all the detected noisy pixels by (i) and (ii), replace each unprocessed noisy pixel p with the median of its $N_p(5)$ including the pixels of previously processed and unprocessed.

The adaptive sequentially weighted median processing, which differentiates accurately the contributions and impacts of neighbor pixels on the central pixel with a sequentially weighted operator, can achieves a better recovery result, and can be capable of restoring the edge and structure information very well.

IV. EXPERIMENTS

By running Matlab R2019a on a machine with Intel(R) Core(TM) i7-7700 CPU at 3.60 GHZ, equipped with 8 GB RAM, we conduct the experiments on datasets *SET12*, *BSD68*, and medical images shown in FIGURE 6. The empirical validation for the proposed ASWMF is conducted by performing thorough comparative analyses with the state-of-the-art filters proposed recently in literatures, which are DAMF [11], NDBINF [13], PVGF [18], ADWMF [22], RBFI [24], SVMFF [25], NAISM [27], and INLM [30], in terms of noise detection accuracy, peak signal to noise ratio (PSNR), structural similarity index (SSIM) [33], edge preservation index (EPI) [34], image entropy H [35], visual perception, and computational time. The PSNR, SSIM, EPI, and H are defined by

$$\text{PSNR} = 10 \times \log_{10} \frac{m \times n \times 255^2}{\sum_{i=1}^m \sum_{j=1}^n (f(i, j) - g(i, j))^2} \tag{8}$$

$$\text{SSIM} = \frac{(2u_f u_g + C_1)(2\sigma_{fg} + C_2)}{(u_f^2 + u_g^2 + C_1)(\sigma_f^2 + \sigma_g^2 + C_2)}, \tag{9}$$

$$(C_1 = (K_1 L)^2, C_2 = (K_2 L)^2)$$

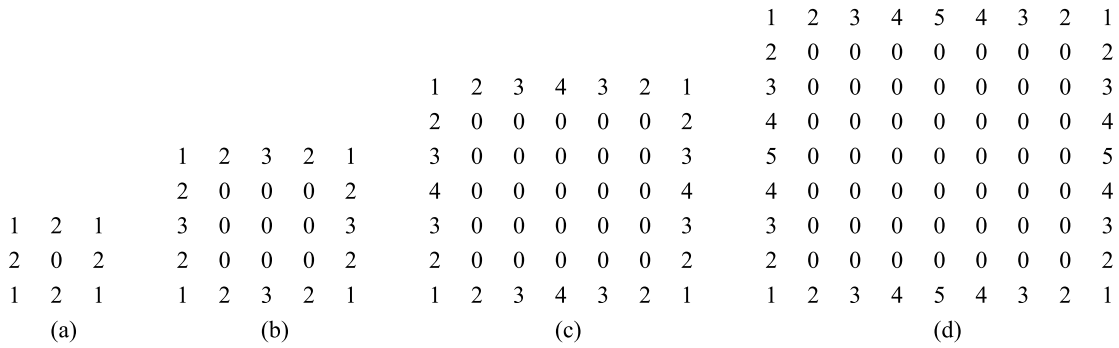


FIGURE 5. Sequentially weighted operator $W(k)$ of (a) size 3×3 ; (b) size 5×5 ; (c) size 7×7 ; (d) size 9×9 .

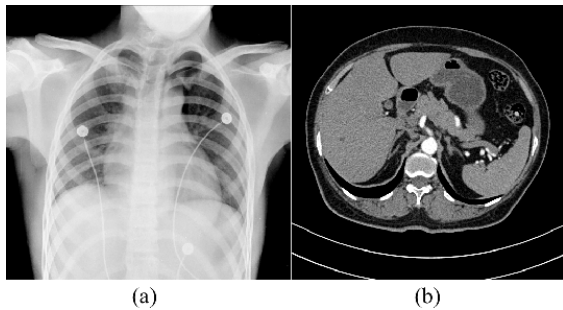


FIGURE 6. Medical images. (a) Chest_Xray; (b) Abdomen_CT.

$$EPI = \frac{\sum_{i=1}^m \sum_{j=1}^n (f_{hp}(i, j) - u_{f_{hp}}) \times (g_{hp}(i, j) - u_{g_{hp}})}{\sqrt{\sum_{i=1}^m \sum_{j=1}^n (f_{hp}(i, j) - u_{f_{hp}})^2 \times \sum_{i=1}^m \sum_{j=1}^n (g_{hp}(i, j) - u_{g_{hp}})^2}} \quad (10)$$

$$H = - \sum_{i=0}^{255} \sum_{j=0}^{255} P_{ij} \ln P_{ij}, \quad \left(\sum_{i=0}^{255} \sum_{j=0}^{255} P_{ij} = 1 \right) \quad (11)$$

Here, f and g are the original image and recovery image, respectively; m and n are the height and width of image, respectively. Denoted by u_f and σ_f the mean and standard deviation of f , respectively, σ_{fg} the covariance of f and g . The stabilizing constant C_1 and C_2 are calculated with the dynamic range, $L = 255$, K_1 and K_2 , by default K_1 and K_2 are selected as 0.01 and 0.03, respectively [33]. f_{hp} and g_{hp} are respectively the high-pass filtering images of f and g with Laplacian filter, with $u_{f_{hp}}$ and $u_{g_{hp}}$ being their mean values, respectively [34]. P_{ij} reflects the comprehensive characteristics of the intensity distribution of one pixel and its surrounding pixels [35].

PSNR measures the similarity of original image and recovery image; the higher the PSNR is, the better the noise removal capability is. SSIM measures the structure information preservation capability; higher SSIM signifies better preservation capability. EPI measures the edge preservation capability; the higher the EPI is, the better the edge preservation capability is. Entropy H is a statistical measure of randomness and variability that can be used to characterize

TABLE 1. Performance of the state-of-the-art filters and ASWMF in noise detection on image Chest_Xray.

Density(%)	10	30	50	70	90
Results:	MDR / FDR(%)				
DAMF	0.00 / 130.	0.00 / 38.7	0.00 / 20.6	0.00 / 12.7	0.00 / 8.38
NDBINF	0.00 / 46.9	0.00 / 28.6	0.00 / 18.5	0.02 / 12.3	0.15 / 8.29
ADWMF	0.00 / 21.3	0.00 / 5.77	0.00 / 2.87	0.00 / 1.54	0.07 / 0.84
SVMFF	0.00 / 7.50	0.00 / 13.3	0.00 / 15.7	0.00 / 12.1	0.01 / 8.34
INLM	0.15 / 42.6	0.18 / 13.5	0.17 / 7.00	0.20 / 4.22	0.20 / 4.23
ASWMF	0.15 / 1.04	0.18 / 0.48	0.17 / 0.42	0.16 / 0.43	0.17 / 1.04

the texture of image; larger entropy implies coarser texture and better texture preservation ability [36].

A. NOISE DETECTION PERFORMANCE OF FILTERS

Among DAMF, NAISM, PVGF, and RBFI, we only take DAMF for evaluation, for they adopt the same noise detection strategy, i.e., min-max noise detector. In terms of missing detection rate (MDR) and false detection rate (FDR), the detected results of all filters on image Chest_Xray are shown in TABLE 1; and the MDR and FDR are given by

$$MDR = 100 \times \frac{\sum_{p \in f} (R_r(p) = 1 \wedge R_d(p) = 0)}{\sum_{p \in f} R_r(p)} (\%) \quad (12)$$

$$FDR = 100 \times \frac{\sum_{p \in f} (R_r(p) = 0 \wedge R_d(p) = 1)}{\sum_{p \in f} R_r(p)} (\%) \quad (13)$$

Here R_r denotes the matrix for indicating the true noises, which indicate a pixel p as noise free with $R_r(p) = 0$ or noisy with $R_r(p) = 1$; R_d denotes the matrix for indicating the detected noises.

By comparing the statistics in TABLE 1, two points can be concluded. (i) At various noise densities, some existing filters have a very small number in MDR, show superiority over the proposed ASWMF; however, they have a very large number in FDR, such as DAMF and SVMFF. (ii) Although the ASWMF shows no superiority in MDR, it achieves

TABLE 2. PSNR and SSIM of the state-of-the-art filters and ASWMF on image Lenna.

Density(%)	10	30	50	70	90	10	30	50	70	90
Filter	PSNR(dB)					SSIM(%)				
DAMF	42.6	36.6	33.0	30.1	25.7	99.7	99.0	97.8	95.4	86.8
NDBINF	42.6	36.6	33.0	29.3	21.7	99.7	99.0	97.7	94.0	73.8
PVGF	42.6	36.6	33.0	29.8	16.2	99.7	99.0	97.8	95.1	45.9
ADWMF	42.0	36.1	32.2	29.5	22.6	99.7	98.9	97.2	94.2	83.0
RBFI	42.2	36.9	33.6	30.5	26.0	99.7	99.1	97.9	95.6	87.1
SVMFF	41.2	34.3	30.0	25.7	19.7	99.7	98.5	95.7	88.1	63.6
NAISM	38.5	33.4	30.9	28.6	25.4	99.5	98.2	96.2	92.9	85.0
INLM	43.3	37.1	33.9	30.6	26.0	99.7	99.1	98.0	95.6	87.1
ASWMF	44.2	38.1	34.4	31.2	27.7	99.8	99.3	98.4	96.4	90.9

a far smaller number in FDR. These imply that ASWMF can achieve better noise detection overall comparing to the other filters at various noise densities.

B. PERFORMANCE OF FILTERS ON SET12 DATASET

Here, the PSNR, SSIM, and EPI of the recovery results of the state-of-the-art filters and ASWMF on images Lenna, Mandrill, Man, and Boat from SET12 dataset, which are corrupted by various density of impulse noise, are tabulated; and the best results are indicated in bold. Applying the proposed ASWMF brings about a considerable increase in the PSNR, SSIM and EPI compared with the state-of-the-art filters with respect to various noise densities.

The results of all filters on image Lenna are tabulated as TABLE 2. It can be inferred from numerical results that the ASWMF gives a considerable improvement in noise removal and structure information preservation at all noise densities; in PSNR, the ASWMF consistently achieves superior results to those of the other filters, and in SSIM, the superiority of ASWMF to the other filters at high noise density is more significant than that at low noise density. These can be attributed to the intelligent use of the 3σ principle of normal distribution and the local intensity statistics in noise detection, as well as the sequentially weighted median processing.

The restored results of all filters for image Mandrill are revealed in TABLE 3. From the PSNR and SSIM values in TABLE 3, it can be easily grasped that the performance of ASWMF is much better than those of the other competing state-of-the-art filters. ASWMF is the most successful method than the others even at high noise density. It is noteworthy that the superiority of ASWMF in SSIM over the other filters grows, as the noise density increases. These imply that the ASWMF is successfully devoted to improving the noise detection, noise removal and structural information preservation.

In terms of PSNR and EPI, the superior performance of ASWMF to the other filters for image Man is demonstrated in TABLE 4. Compared to the state-of-the-art filters,

TABLE 3. PSNR and SSIM of the state-of-the-art filters and ASWMF on image Mandrill.

Density(%)	10	30	50	70	90	10	30	50	70	90
Filter	PSNR(dB)					SSIM(%)				
DAMF	37.8	32.1	28.8	25.9	21.7	99.6	98.4	95.9	90.7	70.9
NDBINF	37.8	32.1	28.8	25.5	19.6	99.6	98.4	95.9	89.8	62.6
PVGF	37.8	32.1	28.8	25.8	15.7	99.6	98.4	95.9	90.6	47.9
ADWMF	37.4	31.2	27.0	24.5	20.5	99.6	97.9	92.7	84.0	66.1
RBFI	38.3	32.9	29.6	26.3	21.9	99.7	98.6	96.3	91.1	71.1
SVMFF	36.8	30.2	25.9	22.4	18.5	99.5	97.3	91.3	76.6	42.9
NAISM	32.3	27.5	25.2	23.4	21.2	98.8	94.9	88.4	78.6	61.2
INLM	40.2	33.5	29.9	26.4	21.9	99.8	98.7	96.6	91.4	71.3
ASWMF	41.0	34.5	30.6	26.9	23.3	99.8	99.1	97.6	93.3	80.4

TABLE 4. PSNR and EPI of the state-of-the-art filters and ASWMF on image Man.

Density(%)	10	30	50	70	90	10	30	50	70	90
Filter	PSNR(dB)					EPI(%)				
DAMF	39.9	34.0	30.7	28.0	24.1	95.4	85.3	72.8	58.1	39.9
NDBINF	39.9	34.0	30.7	27.4	20.9	95.4	85.3	72.8	57.9	37.7
PVGF	39.9	34.0	30.7	27.8	16.0	95.4	85.3	72.8	58.0	32.0
ADWMF	39.3	33.8	30.2	27.6	22.4	95.4	85.1	71.0	55.7	37.2
RBFI	39.3	34.2	31.2	28.3	24.3	94.0	83.1	71.7	57.6	39.7
SVMFF	38.7	32.4	28.3	24.2	19.0	94.8	82.7	67.4	50.6	33.4
NAISM	36.3	31.5	28.9	26.9	24.0	92.3	78.6	65.6	52.8	37.7
INLM	40.5	34.6	31.5	28.4	24.4	95.7	84.7	73.9	59.5	40.1
ASWMF	41.6	35.5	32.1	29.0	25.8	96.5	88.2	77.8	63.4	47.6

the ASWMF gives more promising results; its higher PSNR values imply better noise removal capability, and its higher EPI values signify better edge preservation capability. In PSNR, the superiority of ASWMF to the other filters is almost approximate along various noise densities; and in EPI, the superiority of ASWMF grows, as the noise density increases. This is primarily due to the fact that ASWMF can accurately discriminate the noisy pixels from the noise free ones, and effectively estimate the intensity of noisy pixel, thereby making it more able to restore the image from high density noise.

In terms of PSNR and EPI, TABLE 5 shows the superior results of ASWMF to those of the other filters for image Boat. By observing carefully TABLE 5, we arrived at two conclusions. (i) The ASWMF improve the performance of the existing filters by removing noise thoroughly and rendering the restored image free from blur effect, while the edge information is well preserved. (ii) The superiority of ASWMF to the other filters in EPI increases with the noise

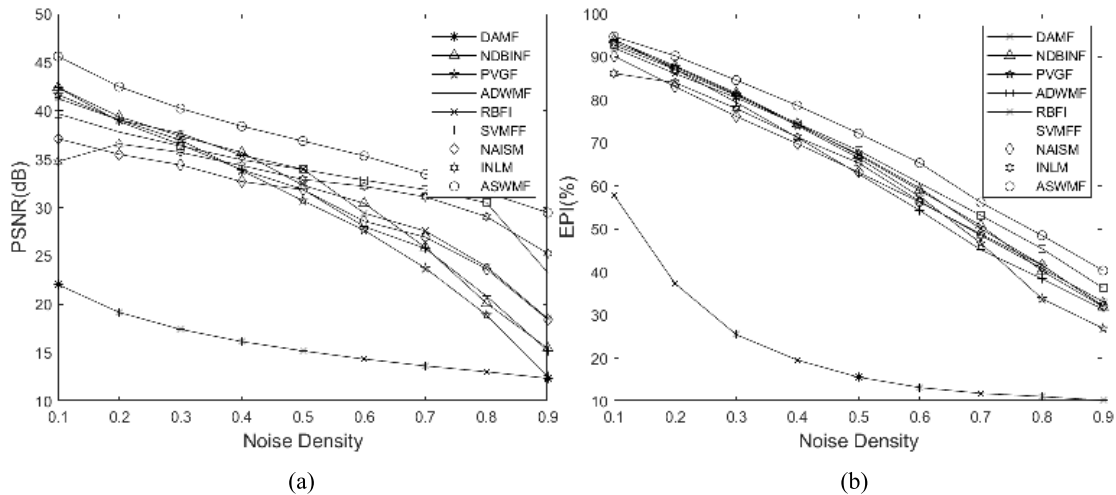


FIGURE 7. PSNR and EPI of the state-of-the-art filters and ASWMF on image chest_Xray. (a)PSNR; (b)EPI.

TABLE 5. PSNR and EPI of the state-of-the-art filters and ASWMF on image boat.

Density(%)	10	30	50	70	90	10	30	50	70	90
Filter	PSNR(dB)					EPI(%)				
DAMF	38.8	32.8	29.5	26.8	23.0	95.0	83.9	70.9	56.0	38.1
NDBINF	38.8	32.8	29.4	26.3	20.3	95.0	83.9	70.9	55.9	37.1
PVGF	38.8	32.8	29.5	26.7	15.8	95.0	83.9	70.9	56.0	32.4
ADWMF	38.2	32.7	29.0	26.4	21.7	95.0	84.0	69.9	54.5	37.2
RBF	38.2	33.1	30.0	27.1	23.2	94.0	82.8	70.6	55.9	38.6
SVMFF	37.7	31.2	27.2	23.4	18.2	94.5	81.7	66.4	49.5	32.9
NAISM	34.7	29.8	27.4	25.4	22.8	92.1	77.6	64.2	50.5	36.4
INLM	39.6	33.5	30.3	27.3	23.2	95.6	84.5	73.0	57.8	39.3
ASWMF	40.4	34.6	31.2	28.0	24.9	96.3	87.5	76.2	61.6	46.5

density increases; thus, the edge information preserved by ASWMF is remarkably better than those preserved through the other filters. These imply that noise removal and edge information preservation can be achieved more effectively by ASWMF.

C. PERFORMANCE OF FILTERS ON MEDICAL IMAGES

Here, we investigate the performance of ASWMF on medical images; and the superiority of ASWMF is revealed by the results plotted in FIGURE 7 and 8. The PSNR and EPI of the recovery results of the state-of-the-art filters and ASWMF on image Chest_Xray with various density of impulse noise, are plotted in FIGURE 7. From FIGURE 7, it is noticed that compared to the other filters, substantial performance improvements can be obtained through ASWMF; the ASWMF outperforms the state-of-the-art filters in noise removal thoroughly which is revealed by PSNR curves. As to the edge information preservation, which is revealed

by EPI curves, the conclusion derived from EPI is similar as that derived from PSNR; along various noise densities, the ASWMF shows excellent performance in edge preservation. The reason behind these improvements is that the ASWMF can accurately discriminate the noisy pixels from the noise free ones, so as to protect the noise free pixels, and effectively remove the noise while preserving the edge information.

FIGURE 8 clearly demonstrates that ASWMF gives definite improvements in PSNR and SSIM over those of the other filters for image Abdomen_CT. Compared to the other filters, the ASWMF shows more promise for processing medical images; in noise removal processing by ASWMF, more structure information can be preserved and better denoising performance can be achieved. Many pixels having extreme intensity are often available in medical images; hence, the superiority of ASWMF over the other filters in medical image processing highly depends on its noise detector.

D. PERFORMANCE OF FILTERS ON BSD68 DATASET

We plot in FIGURE 9 and 10 the average PSNR, SSIM, EPI, and entropy values of the state-of-the-art filters and ASWMF on BSD68 dataset with various density of impulse noise, visualizing their denoising performance.

As expected, the results in FIGURE 9 confirm the superiority of ASWMF again, and are consistent with the results reported above. Three important observations can be made from FIGURE 9. (i) As the noise density increases, consistently for all filters, the restoration quality degenerates, but our method consistently gives the best performance. (ii) The PSNR and SSIM curves of ASWMF are above those of the other filters, keeping a gap with them along various noise densities. (iii) Interestingly and apparently, the performance gap between ASWMF and the other filters in SSIM grows larger, as the noise density increases.

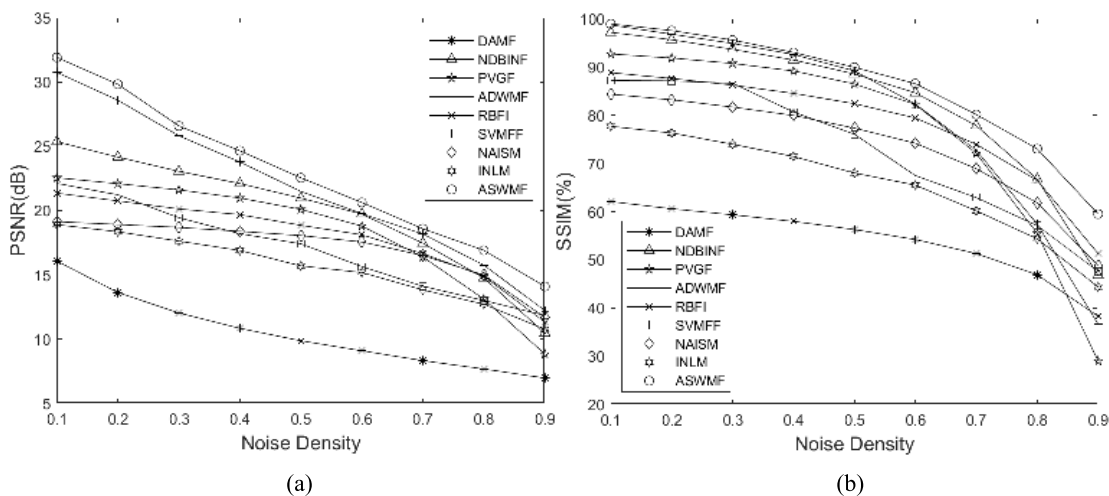


FIGURE 8. PSNR and SSIM of the state-of-the-art filters and ASWMF on image Abdomen_CT. (a) PSNR; (b) SSIM.

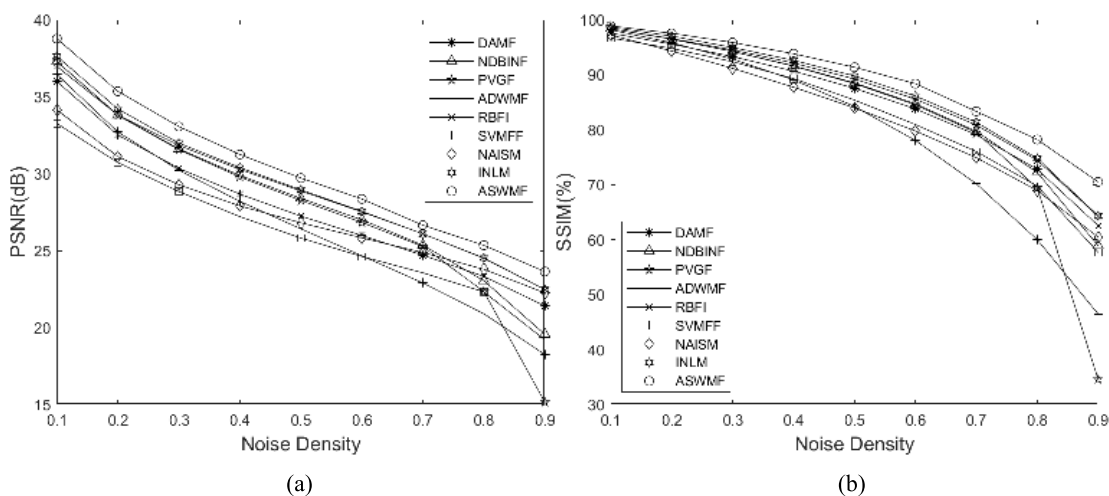


FIGURE 9. Average PSNR and SSIM of the state-of-the-art filters and ASWMF on BSD68 dataset. (a) PSNR; (b) SSIM.

The results in FIGURE 10 confirm the better capability of proposed ASWMF in edge preservation, and keeping the uniformity of image intensity distribution and the image textures. It can be seen obviously that the EPI values of ASWMF are larger than those of other filters along various noise densities, showing better edge preservation capability; as to the entropy of recovery image, the ASWMF outperforms the other filters at almost all the noise densities, except that ASWMF lags behind the DAMF at very high noise density, showing good capability in keeping the variation of image intensity and the image textures.

These can be attributed to that the ASWMF is designed in such a way that it discriminates the noisy pixels accurately from the noise free ones and estimates the intensity of noisy pixel effectively.

E. VISUAL PERCEPTION OF RECOVERY RESULTS

Here, the images Barbara and Jetplane in SET12 are selected as experimental images. Because the performance of a filter

at low noise density is often difficult to evaluate by visual perception, we focus on evaluating it at high noise density. Visual analyses on the capability of noise removal, structure and edge information preservation of the proposed ASWMF against the state-of-the-art filters in the recovery results for image Barbara with 80% impulse noises and Jetplane with 90% impulse noises are made in FIGURE 11 and 12, respectively. For a visually clear comparison, only a zoomed-in local part of each recovery image is shown.

FIGURE 11 shows the improvements in visual appearance given by ASWMF against the state-of-the-art filters for image Barbara; two numbers in the parentheses below each recovery image are the corresponding PSNR and SSIM, respectively. By observing FIGURE 11 carefully, three important conclusions can be inferred. (i) The ASWMF gives a more visually pleasant recovery image, and provides a significant contribution towards preserving the structural information. (ii) In the recovery images of the other filters, either residual noises or obvious blur effects can be seen.

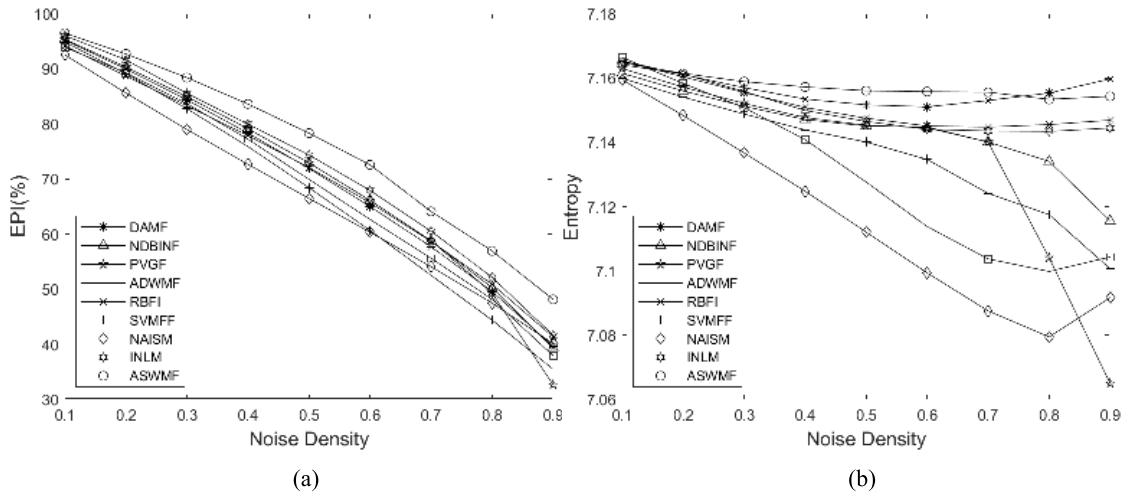


FIGURE 10. Average EPI and entropy of the state-of-the-art filters and ASWMF on BSD68 dataset. (a)EPI; (b)Entropy.



FIGURE 11. Recovery results of image Barbara with 80% impulse noises.(a) Zoomed-in local part of Barbara with impulse noise; Results of (b) DAMF; (c) NDBINF; (d) PVGF; (e) ADWMF; (f) RBF1; (g) SVMFF; (h) NAISM; (i) INLM; (j) ASWMF.

(iii) Again, the PSNR and SSIM values below the recovery images confirm the superiority of ASWMF over the other filters. These mean that the ASWMF possesses better capability of noise removal and structural information preservation than the existing filters, and the image produced by the ASWMF is visually sharper and more distinctive than those obtained by the other filters.

The recovery images of all filters on image Jetplane with 90% impulse noises, are shown in FIGURE 12; two numbers in the parentheses below each recovery image are the corresponding PSNR and EPI, respectively. On careful observation from FIGURE 12, the visual result of ASWMF is perceptually better than those of the other considered filters; the recovery results confirm that our result is far superior to those of the other filters, indicating that the ASWMF still produces consistently higher quality image at such a high corruption

level with better capability of local features preservation. And the corresponding PSNR and EPI are also consistent with the conclusion derived by visual perception. The ASWMF still works fairly well, even at a very high noise density; this is due to the same reason as explained above.

Here, these inferences by visual perception are consistent with the comments given above.

F. COMPUTATIONAL TIME

Denoted by n the pixel number of one image and C_x a constant. Consider the complexity of each subprocess in the proposed ASWMF: noise detection by extreme intensity— $O(n)$; detection by 3σ principle or local intensity statistics— $O(C_1n)$, here $C_1 = 49$ or $C_1 = 25$; search noise free pixels in neighborhood of adaptive size— $O(C_2n)$; weighted processing for each noisy

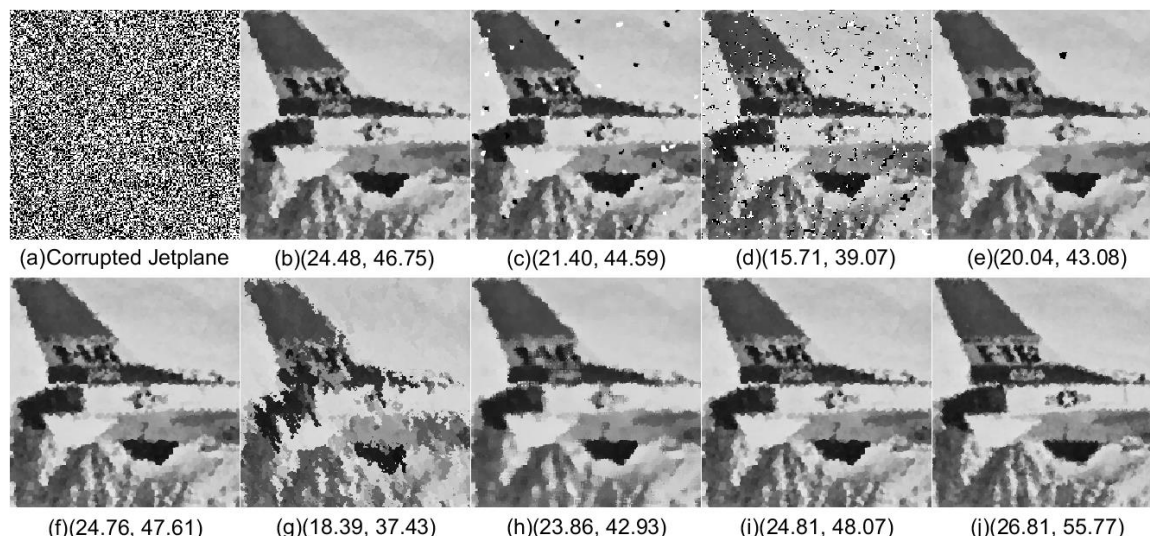


FIGURE 12. Recovery results of image Jetplane with 90% impulse noises. (a) Zoomed-in local part of Jetplane with impulse noise; Results of (b) DAMF; (c) NDBINF; (d) PVGF; (e) ADWMMF; (f) RBFI; (g) SVMFF; (h) NAISM; (i) INLM; (j) ASWMMF.

TABLE 6. Average computational time (seconds) of each filter on six selected images.

Density(%)	10	20	30	40	50	60	70	80	90
DAM	0.13	0.24	0.33	0.44	0.56	0.68	0.79	0.92	1.13
NDBINF	0.41	0.50	0.62	0.71	0.88	0.95	1.03	1.21	1.39
PVGF	0.12	0.23	0.32	0.43	0.56	0.67	0.77	0.93	1.06
ADWMMF	17.3	34.3	66.2	102.	170.	241.	300.	340.	382.
RBFI	6.13	12.1	17.2	22.4	26.6	32.5	34.7	37.7	44.6
SVMFF	3.23	3.85	4.14	4.55	4.97	5.49	5.91	6.27	6.72
NAISM	2.42	4.09	5.81	8.19	10.0	12.4	14.9	17.1	23.1
INLM	16.3	35.4	55.0	72.4	82.3	92.2	101.	105.	107.
ASWMMF	1.83	2.94	4.96	6.28	7.56	9.99	12.5	16.7	20.3

pixel— $O(C_3n)$; replace each noisy pixel with median— $O(C_4n)$. Therefore, summing them together, the total complexity of ASWMMF is $O((1+C_1+C_2+C_3)n)$. Hence, it can be concluded that the computational complexity of the proposed ASWMMF is acceptable. Further, we end this section by considering the computational time of our ASWMMF and the state-of-the-art filters; they are performed on image Lenna, Mandril, Man, Boat, Barbara, and Jetplane, and the average computational time of each filter is tabulated as TABLE 6.

A careful look at TABLE 6 and reference to the above performance analyses reveal that some state-of-the-art filters often provide such a good performance only at the cost of computational time, such as INLM and RBFI. Among all filters, no significant superiority in computational time is shown by the proposed ASWMMF; however, its running speed is comparable to most of the state-of-the-art filters, and surpasses some other filters, such as ADWMMF, INLM and RBFI.

V. CONCLUSION

In this paper, we proposed a new method ASWMMF for image restoration from impulse noise, consisting of a simple and effective noise detector, and a noise removal technique capable of removing impulse noise thoroughly and preserving the structure and edge information very well. The noise detector in ASWMMF takes full advantage of the 3σ principle of normal distribution and the local intensity statistics; and the noise removal technique in ASWMMF gets support from the adaptive sequentially weighted median processing. The 3σ principle of normal distribution and local intensity statistics employed in noise detection and the adaptive sequentially weighted operator employed in noise removal are the remarkable contributions of the proposed ASWMMF; they jointly make the denoising performance advanced considerably. With extensive experimental results on various images with various density of impulse noise, it is observed that quantitatively and qualitatively, the proposed ASWMMF performs superiorly to the state-of-the-art filters in the presence of impulse noise. In addition, no significant superiority in computational time is shown by the proposed ASWMMF; we will advance it in the further work, making it applicable for real-time image denoising.

ACKNOWLEDGMENT

The authors would like to thank the editors and anonymous reviewers for their constructive suggestions to the improvements of this article.

REFERENCES

[1] K. H. Jin and J. C. Ye, “Sparse and low-rank decomposition of a Hankel structured matrix for impulse noise removal,” *IEEE Trans. Image Process.*, vol. 27, no. 3, pp. 1448–1461, Mar. 2018.
 [2] L. Liu, C. P. Chen, Y. Zhou, and X. You, “A new weighted mean filter with a two-phase detector for removing impulse noise,” *Inf. Sci.*, vol. 315, pp. 1–16, Sep. 2015.

- [3] W. Ye, "Optimality of the median filtering operator," *Circuits, Syst. Signal Process.*, vol. 30, no. 6, pp. 1329–1340, 2011.
- [4] N. Singh and U. Oorkavalan, "Triple threshold statistical detection filter for removing high density random-valued impulse noise in images," *EURASIP J. Image Video Process.*, vol. 2018, no. 1, p. 22, 2018.
- [5] M. S. Nair and P. M. A. Mol, "Direction based adaptive weighted switching median filter for removing high density impulse noise," *Comput. Electr. Eng.*, vol. 39, no. 2, pp. 663–689, 2013.
- [6] C. Yuan and Y. Li, "Switching median and morphological filter for impulse noise removal from digital images," *Optik*, vol. 126, no. 18, pp. 1598–1601, 2015.
- [7] A. S. Awad, "Standard deviation for obtaining the optimal direction in the removal of impulse noise," *IEEE Signal Process. Lett.*, vol. 18, no. 7, pp. 407–410, Jul. 2011.
- [8] S. K. Meher and B. Singhawat, "An improved recursive and adaptive median filter for high density impulse noise," *Int. J. Electron. Commun.*, vol. 68, no. 12, pp. 1173–1179, 2014.
- [9] J. Y. Lee, S. Y. Jung, and P. W. Kim, "Adaptive switching filter for impulse noise removal in digital content," *Soft Comput.*, vol. 22, no. 5, pp. 1445–1455, 2017.
- [10] Y. Wang, J. Fu, H. Dihn, and R. Adhami, "A novel learning-based switching median filter for suppression of impulse noise in highly corrupted colour images," *Imag. Sci. J.*, vol. 64, no. 1, pp. 15–25, 2016.
- [11] U. Erkan, L. Gökrem, and S. Enginoğlu, "Different applied median filter in salt and pepper noise," *Comput. Electr. Eng.*, vol. 70, pp. 789–798, Aug. 2018.
- [12] S. Esakirajan, T. Veerakumar, A. N. Subramanyam, and C. H. Premchand, "Removal of high density salt and pepper noise through modified decision based unsymmetric trimmed median filter," *IEEE Signal Process. Lett.*, vol. 18, no. 5, pp. 287–290, May 2011.
- [13] A. K. Samantaray, P. Kanungo, and B. Mohanty, "Neighborhood decision based impulse noise filter," *IET Image Process.*, vol. 12, no. 7, pp. 1222–1227, 2018.
- [14] Z. Li, G. Liu, Y. Cheng, and Y. Xu, "Modified directional weighted filter for removal of salt & pepper noise," *Pattern Recognit. Lett.*, vol. 40, pp. 113–120, Apr. 2014.
- [15] Q.-Q. Chen, M.-H. Hung, and F. M. Zou, "Effective and adaptive algorithm for pepper-and-salt noise removal," *IET Image Process.*, vol. 11, no. 9, pp. 709–716, 2017.
- [16] V. R. Vijaykumar, G. S. Mari, and D. Ebenezer, "Fast switching based median-mean filter for high density salt and pepper noise removal," *AEU-Int. J. Electron. Commun.*, vol. 68, no. 12, pp. 1145–1155, 2014.
- [17] G. Gao and Y. Liu, "An efficient three-stage approach for removing salt & pepper noise from digital images," *Optik*, vol. 126, no. 4, pp. 467–471, 2015.
- [18] C.-T. Lu, M.-Y. Chen, L.-L. Wang, C.-C. Hsu, and J.-H. Shen, "Removal of salt-and-pepper noise for X-ray bio-images using pixel-variation gain factors," *Comput. Electr. Eng.*, vol. 71, pp. 862–876, Oct. 2018.
- [19] M. S. Nair and P. M. A. Mol, "An efficient adaptive weighted switching median filter for removing high density impulse noise," *J. Inst. India, B*, vol. 95, no. 3, pp. 255–278, 2014.
- [20] H. Hosseini, F. Hesar, and F. Marvasti, "Real-time impulse noise suppression from images using an efficient weighted-average filtering," *IEEE Signal Process. Lett.*, vol. 22, no. 8, pp. 1050–1054, Aug. 2015.
- [21] V. Kishorebabu, G. Packyanathan, V. Shankar, and H. Kamatham, "An adaptive decision based interpolation scheme for the removal of high density salt and pepper noise in images," *EURASIP J. Image Video Process.*, vol. 2017, no. 1, 2017, Art. no. 67.
- [22] S. Khan and D.-H. Lee, "An adaptive dynamically weighted median filter for impulse noise removal," *EURASIP J. Adv. Signal Process.*, vol. 2017, Sep. 2017, Art. no. 67.
- [23] Y. Wang, J. Wang, S. Xiao, and L. Han, "An efficient adaptive fuzzy switching weighted mean filter for salt-and-pepper noise removal," *IEEE Signal Process. Lett.*, vol. 23, no. 11, pp. 1582–1586, Nov. 2016.
- [24] F. Taherkhani and M. Jamzad, "Restoring highly corrupted images by impulse noise using radial basis functions interpolation," *IET Image Process.*, vol. 12, no. 1, pp. 20–30, 2018.
- [25] A. Roy, J. Singha, S. S. Devi, and R. H. Laskar, "Impulse noise removal using SVM classification based fuzzy filter from gray scale images," *Signal Process.*, vol. 128, pp. 262–273, Apr. 2016.
- [26] M. Habib, A. Hussain, M. Ali, and S. Rasheed, "Adaptive fuzzy inference system based directional median filter for impulse noise removal," *AEU-Int. J. Electron. Commun.*, vol. 70, no. 5, pp. 689–697, 2016.
- [27] S. Arora, M. Hanmandlu, and G. Gupta, "Filtering impulse noise in medical images using information sets," *Pattern Recognit. Lett.*, to be published, doi: 10.1016/j.patrec.2018.06.002.
- [28] M. González-Hidalgo, S. Massanet, D. Ruiz-Aguilera, and A. Mir, "Improving salt and pepper noise removal using a fuzzy mathematical morphology-based filter," *Appl. Soft Comput.*, vol. 63, pp. 167–180, Feb. 2018.
- [29] P. Nair and K. N. Chaudhury, "Fast high-dimensional bilateral and non-local means filtering," *IEEE Trans. Image Process.*, vol. 28, no. 3, pp. 1470–1481, Mar. 2019.
- [30] X. Wang, S. Shen, Y. Xu, P. Zhang, and G. Shi, "Iterative non-local means filter for salt and pepper noise removal," *J. Vis. Commun. Image Represent.*, vol. 38, pp. 440–450, Jul. 2016.
- [31] H. C. Burger, C. J. Schuler, and S. Harmeling, "Image denoising with multi-layer perceptrons, part 1: Comparison with existing algorithms and with bounds," *Comput. Sci.*, Nov. 2012, arXiv:1211.1544. [Online]. Available: <https://arxiv.org/abs/1211.1544>
- [32] S. Harmeling, C. J. Schuler, and H. C. Burger, "Image denoising: Can plain neural networks compete with BM3D?" in *Proc. IEEE Conf. Comput. Vis. Pattern Recognit.*, Jun. 2012, pp. 2392–2399.
- [33] Z. Wang, A. C. Bovik, H. R. Sheikh, and E. P. Simoncelli, "Image quality assessment: From error visibility to structural similarity," *IEEE Trans. Image Process.*, vol. 13, no. 4, pp. 600–612, Apr. 2004.
- [34] V. Soni, A. K. Bhandari, A. Kumar, and G. K. Singh, "Improved sub-band adaptive thresholding function for denoising of satellite image based on evolutionary algorithms," *IET Signal Process.*, vol. 7, no. 8, pp. 720–730, 2013.
- [35] S. Zhang, Y. Liu, and X. Li, "Fast entropy minimization based autofocusing technique for ISAR imaging," *IEEE Trans. Signal Process.*, vol. 63, no. 13, pp. 3425–3434, Jul. 2015.
- [36] R. C. Gonzalez and R. E. Woods, *Digital Image Processing*, 3rd ed. Beijing, China: Electronic Industry Press, 2017.



JIAYI CHEN was born in 1983. He received the M.S. degree in computer science and technology from the Guangdong University of Technology, Guangzhou, China, in 2010. He is an Associate Professor with Guangdong Medical University, Zhanjiang, China. He has published more than 30 articles in his research areas. His research interests include wavelet analysis, signal processing, and image processing.



YINWEI ZHAN (M'12) was born in 1966. He received the M.S. degree in applied mathematics from Jilin University, Jilin, China, in 1989, and the Ph.D. degree in applied mathematics from the Dalian University of Technology, Dalian, China, in 1992. He is a Professor and a M.S. Supervisor with the Guangdong University of Technology, Guangzhou, China. He has published more than 100 articles in his research areas. His research interests include image processing, wavelet analysis, pattern recognition, and computer vision.



HUIYING CAO was born in 1975. She received the M.S. degree in applied electronics from Guangxi Normal University, Guangxi, China, in 2009, and the Ph.D. degree in physics from Nanjing University, Nanjing, China, in 2012. She is an Associate Professor with Guangdong Medical University, Zhanjiang, China. She has published more than 20 articles in her research areas. Her research interests include physical nano materials and image processing.

• • •